A transchromosomic rat model with human chromosome 21 shows robust Down syndrome features

Authors

Yasuhiro Kazuki, Feng J. Gao, Miho Yamakawa, ..., Joan T. Richtsmeier, Mitsuo Oshimura, Roger H. Reeves

Correspondence

rreeves@jhmi.edu (R.H.R.),
kazuki@tottori-u.ac.jp (Y.K.)

Kazuki et al., 2022, The American Journal of Human Genetics *109*, 328–344
February 3, 2022
https://doi.org/10.1016/j.ajhg.2021.12.015

CellPress

ARTICLE

A transchromosomic rat model with human chromosome 21 shows robust Down syndrome features

Yasuhiro Kazuki,[1,2,15,*] Feng J. Gao,[3,15] Miho Yamakawa,[2] Masumi Hirabayashi,[4] Kanako Kazuki,[2] Naoyo Kajitani,[2] Sachiko Miyagawa-Tomita,[5,6] Satoshi Abe,[7] Makoto Sanbo,[4] Hiromasa Hara,[4,16] Hiroshi Kuniishi,[8] Satoshi Ichisaka,[8] Yoshio Hata,[8] Moeka Koshima,[1] Haruka Takayama,[7] Shoko Takehara,[7] Yuji Nakayama,[9] Masaharu Hiratsuka,[1] Yuichi Iida,[2,17] Satoko Matsukura,[10] Naohiro Noda,[10] Yicong Li,[3] Anna J. Moyer,[3] Bei Cheng,[11] Nandini Singh,[12] Joan T. Richtsmeier,[13] Mitsuo Oshimura,[2,7] and Roger H. Reeves[3,14,*]

Summary

Progress in earlier detection and clinical management has increased life expectancy and quality of life in people with Down syndrome (DS). However, no drug has been approved to help individuals with DS live independently and fully. Although rat models could support more robust physiological, behavioral, and toxicology analysis than mouse models during preclinical validation, no DS rat model is available as a result of technical challenges. We developed a transchromosomic rat model of DS, TcHSA21rat, which contains a freely segregating, EGFP-inserted, human chromosome 21 (HSA21) with >93% of its protein-coding genes. RNA-seq of neonatal forebrains demonstrates that TcHSA21rat expresses HSA21 genes and has an imbalance in global gene expression. Using EGFP as a marker for trisomic cells, flow cytometry analyses of peripheral blood cells from 361 adult TcHSA21rat animals show that 81% of animals retain HSA21 in >80% of cells, the criterion for a "Down syndrome karyotype" in people. TcHSA21rat exhibits learning and memory deficits and shows increased anxiety and hyperactivity. TcHSA21rat recapitulates well-characterized DS brain morphology, including smaller brain volume and reduced cerebellar size. In addition, the rat model shows reduced cerebellar foliation, which is not observed in DS mouse models. Moreover, TcHSA21rat exhibits anomalies in craniofacial morphology, heart development, husbandry, and stature. TcHSA21rat is a robust DS animal model that can facilitate DS basic research and provide a unique tool for preclinical validation to accelerate DS drug development.

Introduction

Down syndrome (DS), caused by trisomy for human chromosome 21 (HSA21), is the most common viable aneuploidy and occurs in ~1/800 live births.[1] People with DS have varying levels of intellectual disability. They are at high risk of developing other health conditions, such as congenital heart defects (CHDs), hearing and vision loss, leukemia, gastrointestinal disease, and early-onset dementia.[2,3] Significant progress in prenatal detection, symptom management, and awareness of DS has substantially increased life expectancy and quality of life in people with DS.[3,4] However, most people with DS cannot live independently. Pharmacological approaches to ameliorate different aspects of this complex genetic condition, many tested in mouse models, hold promise, but further research exploring DS mechanisms in optimal model systems is necessary to advance treatments.

HSA21 comprises 46.7 million base pairs (Mb) of DNA (GRCh38.p12). Seventeen and 213 protein-coding genes (PCGs) are annotated in the short arm (HSA21p) and long arm (HSA21q), respectively, in addition to 601 annotated non-PCGs. Trisomy changes expression for HSA21 genes at dosage imbalance with the consequence of genome-wide expression imbalance.[3,5] The first viable DS mouse model, Ts65Dn, contains an extra freely segregating chromosome with 92 of 160 non-keratin associated protein (non-*KRTAP*) genes orthologous to HSA21 and shows features comparable to various DS manifestations, including cognitive impairment, retrusion of the midface

[1]Division of Genome and Cellular Functions, Department of Molecular and Cellular Biology, School of Life Science, Faculty of Medicine, Tottori University, 86 Nishi-cho, Yonago, Tottori 683-8503, Japan; [2]Chromosome Engineering Research Center, Tottori University, Yonago, Tottori 683-8503, Japan; [3]Department of Physiology, Johns Hopkins University School of Medicine, Baltimore, MD 21205, USA; [4]Center for Genetic Analysis of Behavior, National Institute for Physiological Sciences, Okazaki, Aichi 444-8787, Japan; [5]Department of Animal Nursing Science, Yamazaki University of Animal Health Technology, Hachioji, Tokyo 192-0364, Japan; [6]Department of Physiological Chemistry and Metabolism, Graduate School of Medicine, The University of Tokyo, Bunkyo-ku, Tokyo 113-0033, Japan; [7]Trans Chromosomics, Inc., 86 Nishi-cho, Yonago, Tottori 683-8503, Japan; [8]Division of Neuroscience, School of Life Science, Faculty of Medicine, Tottori University, 86 Nishi-cho, Yonago, Tottori 683-8503, Japan; [9]Division of Radioisotope Science, Research Initiative Center, Organization for Research Initiative and Promotion, Tottori University, 86 Nishi-cho, Yonago, Tottori 683-8503, Japan; [10]Biomedical Research Institute, National Institute of Advanced Industrial Science and Technology, Tsukuba, Ibaraki 305-8566, Japan; [11]Department of Radiology, Johns Hopkins University School of Medicine, Baltimore, MD 21205, USA; [12]Department of Anthropology, California State University, Sacramento, CA 95819, USA; [13]Department of Anthropology, Penn State University, State College, PA 16802, USA; [14]Department of Genetic Medicine, Johns Hopkins University School of Medicine, Baltimore, MD 21205, USA
[15]These authors contributed equally
[16]Present address: Center for Molecular Medicine, Jichi Medical University, Tochigi, Japan
[17]Present address: Department of Immunology, Faculty of Medicine, Shimane University, Shimane, Japan
*Correspondence: rreeves@jhmi.edu (R.H.R.), kazuki@tottori-u.ac.jp (Y.K.)
https://doi.org/10.1016/j.ajhg.2021.12.015.

skeleton, resistance to solid tumors, and cerebellar hypoplasia.[6–9]

An optimal genetic model for DS should reflect the conditions in people and would include the following: (1) aneuploidy, an extra freely segregating chromosome introducing an extra centromere into every cell; (2) a large fraction of trisomic HSA21 orthologous genes; (3) few or no trisomic genes that are not HSA21 genes/orthologs; (4) no regions of monosomy, as can occur in translocations;[10] and (5) minimal mosaicism. Ts65Dn contains a freely segregating chromosome but is trisomic for a number of non-HSA21 orthologs.[10,11] Models with direct duplications of conserved regions, such as Dp(16)1Yey, do not have an extra chromosome and centromere.[12,13] Tc1 was the first transchromosomic aneuploid model and is trisomic for a somewhat rearranged HSA21 carrying ~75% of PCGs but shows extensive mosaicism.[14] TcMAC21 is currently the most complete genetic mouse model of DS and contains a hybrid chromosome "HSA21q-MAC" composed of a mouse artificial chromosome (MAC) vector engineered with HSA21q.[15] TcMAC21 has little or no mosaicism and carries 93% of HSA21 PCGs and no non-HSA21 human genes.

A study of 59 new FDA-approved drugs from 2015 to 2016 reported that placebo-controlled or drug comparator clinical trials have an average cost of $35.1 million.[16] Drugs for treating central nervous system disorders have low approval rates.[17] The use of trisomic DS mouse models has identified several potential therapeutic candidates to improve learning and memory in people with trisomy 21.[18–22] Animal models that support more robust physiological and behavioral analysis will provide an essential layer of preclinical validation and have improved outcomes for drug development.

The laboratory rat, *Rattus norvegicus*, was the first mammalian species domesticated for scientific research in 1828 and was the third mammal with a complete genome sequence.[23] Humans and rodents separated from a common ancestor ~75 million years (Myr) ago, while mice and rats diverged ~12–24 Myr.[23–25] Rats have 21 pairs of chromosomes, compared with 23 in humans and 20 in mice. The rat genome (Rnor_6.0) comprises ~2.87 gigabases (Gb), somewhat smaller than the human genome (~3.1 Gb, GRCh38.p12) and slightly larger than the mouse genome (2.73 Gb, GRCm38.p6). The larger body and organ size of rats permits better imaging and surgical/physiological interventions than in mice. Rat organ morphology including cerebellar foliation is more similar to the human than is that of the mouse.[26] Rat behaviors are well characterized and nuanced, including more affiliative social behavior, and rats are generally competent in and less stressed by cognitive tests like the Morris water maze (MWM).[27,28] Moreover, rats are the predominant model system in safety and toxicology studies of new compounds or nutrients. However, there are significant challenges associated with rat transgenesis, particularly for the insertion of large genomic fragments required for DS model generation.[29] Here, we developed and characterized the transchromosomic (Tc) rat model of DS, "TcHSA21rat," which contains a substantially intact and freely segregating EGFP-labeled HSA21 and recapitulates many phenotypes associated with DS.

Material and methods

Generation of rat ES cell line with HSA21

The HSA21-EGFP was constructed with a previously described Cre-loxP-mediated gene insertion system with the HSA21.[30] A loxP site was inserted at position 13,021,348–13,028,858, GenBank: NC_000021.9, in a HSA21 in DT40 cells as described previously.[31] The modified HSA21 (HSA21-loxP) was transferred to CHO cells via MMCT as described previously.[32] HPRT-deficient CHO cells (CHO HPRT$^{-/-}$) containing HSA21 were maintained in Ham's F-12 nutrient mixture. A plasmid vector containing the EGFP flanked by HS4 insulator, loxP and 3′HPRT (I-EGFP-I-loxP-3′HPRT), and Cre-recombinase expression vectors were transfected into CHO cells containing the HSA21-loxP with Lipofectamine 2000. The cell culture and colony expansion were performed as described previously.[31] The site-specific EGFP insertion into the HSA21-loxP was confirmed by PCR and FISH analyses as described previously.[31] To generate the rat ES (HSA21-EGFP) cells, we fused rat ES cells with microcells prepared from the donor CHO hybrid cells containing the HSA21-EGFP and selected them with G418 as described previously.[30] The rBLK2i-1 embryonic stem cell line (RGD: 10054010) was used in this study.

Generation of chimeric and Tc rat

Chimeric rats were generated by blastocyst injection of the rat ES (HSA21-EGFP) cells, as described previously.[33] Briefly, 8–10 cells were microinjected into the blastocoelic cavity of host Crlj:WI (Charles River Laboratories Japan, Kanagawa, Japan) blastocysts. The re-blastulated embryos were transferred into the uteri of pseudopregnant Crlj:WI recipients to allow the full-term development to pups. The contribution of the ES cells in the resultant offspring was confirmed by their coat color and/or the GFP fluorescence. To examine the germline competency of the chimera to the F1 generation, we applied round spermatid injection (ROSI)[34] with a few modifications. At 10 weeks old, testes of chimeras were microdissected, and GFP-positive seminiferous tubules (Figure S1D) were selected for ROSI. Round spermatids were FACS-sorted from the testicular cell suspension after a freeze-thaw procedure. Oocytes retrieved from superovulated Slc:SD (Japan SLC, Shizuoka, Japan) female rats at 4–5 weeks old were activated with 5 μM ionomycin in mR1ECM for 5 min and were cultured in mR1ECM for 40 min. Then, these oocytes were injected with the round spermatid followed by an additional culture in mR1ECM for 20 min and 5 μg/mL cycloheximide in mR1ECM for 4 h. The next morning, the ROSI oocytes were transferred into the oviducts of pseudopregnant Crlj:WI recipients and pups were examined for GFP expression.

Animals

All procedures related to animal care and treatment were approved by each local university/institutional animal care and use committee, and the procedures followed were in accordance with the ethical standards of the committee on animal experimentation. TcHSA21rats and TcMAC21 mice were maintained on Wistar

(Crlj:WI, Charles River) and BDF1 (C57BL/6J (B6) x DBA/2J (D2)), respectively. Rats and mice were maintained in a Tottori University animal facility with 12 h light/12 h dark cycle and temperatures of 20°C–26°C with 40%–70% humidity and were fed with standard chow and in-cage automatic water.

ARRIVE guidelines were followed in the design and execution of the project. A consolidated table of demographic animal information for each experiment of each figure, including genetic background, age, gender, and sample size, is provided (Table S1). Investigators were blind to sample genotypes in all assays.

FISH analyses

FISH was performed with fixed metaphase or interphase spreads. Slides were hybridized with digoxigenin (or biotin)-labeled (Roche, Basel, Switzerland) human COT-1 DNA (Thermo Fisher) to detect HSA21 and biotin-labeled I-EGFP-I-loxP-3′HPRT (Thermo Fisher) to detect EGFP on the HSA21, essentially as described previously.[32,35]

Whole-genome sequencing (WGS)

Tail DNA from two TcHSA21rats was purified and sequenced for two different runs with the Illumina NextSeq 500 system. A library prepared with TruSeq DNA PCR-Free LT Sample Prep Kit (Illumina, USA) was used for the first run, and a library prepared with Nextera Mate Pair Sample Prep Kit (Illumina) was used for the second run. After cleaning the sequence reads, the short reads were mapped to whole-genome sequences of rat (NCBI Rnor_6.0) and human chromosome 21 (GenBank: NC_000021.9) with CLC Genomics Workbench ver. 9.5. A total of 536 million reads were mapped to the reference genome. Among those reads, 3.8 million reads were mapped to HSA21, GRCh38.p13 Primary Assembly. Excluding zero coverage regions, the effective depth of coverage was 16.7×.

RNA sequencing (RNA-seq)

RNA was extracted from forebrains of GFP-negative euploid (Eu) and GFP-positive TcHSA21rat males (n = 3 per group) at P1. Standard mRNA purification and library preparation were conducted using NEBNext Poly (A) mRNA Magnetic Isolation (E7490) and NEBNext Ultra II RNA Library Prep Kit (E7770). Library quality was assessed via Agilent 2100 Bioanalyzer for DNA High sensitivity DNA chip. The prepared library was sequenced with HiSeq2500 Flowcell with 100 bp paired-end reads, and each sample contained approximately 50–60 million reads. We assessed the sequences with fastqc and trimmed 30 bp from each sequence to achieve higher accuracy. We extracted HSA21 reference and appended it onto the whole rat genome reference sequence to create the modified reference. Reads were then aligned with TopHat2. Sim4 and Leaff were used for cross-species analysis. Standard DEseq methodology was used for differential gene expression analysis.

Flow cytometry

To evaluate the percentage of GFP-expressing cells by flow cytometry (FCM), we collected peripheral blood cells from TcMAC21 mice and TcHSA21rats through tail vein and treated them with ammonium chloride solution (0.17 M NH_4Cl in distilled water) for hemolysis followed by FCM buffer (5% FBS/1 mM EDTA in PBS) substitution. Resuspended cells were filtrated with 40 μm pore cell strainers, and the levels of GFP expression were analyzed by Gallios (Beckman Coulter). Cells were illuminated with a 488 nm laser, and the fluorescence was detected with the FL1 525 ± 40 nm bandpass filter. Peripheral blood mononuclear cells (PBMCs) were gated for analysis, and minimal 20,000 events in the gate were analyzed. The same GFP-positive gating was used for each group to differentiate GFP-positive and -negative cells. The percentage of GFP-positive (GFP^+) cells was calculated by the number of GFP-positive cells within PBMCs in the gate.

To evaluate the percentage of GFP-expressing cells in lymphocyte subsets, we collected peripheral blood cells and spleen from TcHSA21rats euthanized with isoflurane. Peripheral blood cells were stained with cell-type-specific antibodies, and additional samples were prepared by staining with corresponding isotype control antibodies. Cells were hemolyzed, washed with FCM buffer, and filtered with cell strainers for FCM analysis. The spleen was physically processed by mashing between the frosted ends of two glass slides, and dissociated cells were resuspended with 10 mL of FCM buffer and filtered with 40 μm pore cell strainers. Cells were hemolyzed, resuspended with 10 mL of FCM buffer, filtered through 40 μm pore cell strainers, and counted. For staining, 1×10^6 cells were applied to each reaction and incubated on ice for 30 min, followed by washing with FCM buffer and filtration. Antibodies used in this assay were mouse anti-rat CD45RA (OX-33, Biolegend), CD161 (10/78, eBioscience), CD3 (1F4, Biolegend), CD4 (W3/25, Biolegend), CD8a (OX-8, Biolegend), and CD45R (HIS24, BD PharMingen) conjugated with PE, PerCP-eFluor710, Alexa Fluor 647, PE, PerCP, and PE, respectively. FCM analysis was performed with Gallios with different combinations of laser (488 nm and 638 nm) and bandpass filter (FL1 525 ± 40, FL2 575 ± 30, FL4 695 ± 30 for PerCP-eFluor710 or 675 ± 10 for PerCP, and FL6 660 ± 20 nm). The lymphocyte population was gated, and >13,000 cells were analyzed. Positive and negative populations were determined with samples stained by isotype controls. The percentage of GFP-positive cells in each lymphocyte subset was calculated by the number of GFP-positive cells within the subset.

Behavioral analyses

Experimental design

Rats used for behavioral tests were male F6-8 TcHSA21rat on Wistar background. Blood cells of GFP-positive and GFP-negative littermates were collected from tail veins at 3–5 weeks of age, and GFP-positive cell rates of PBMCs were analyzed by flow cytometry. TcHSA21rats with >80% GFP-positive rates (TcHSA21rat, n = 15) and GFP-negative littermates (Eu rats, n = 15) were used. Each rat was handled by experimenters for 5 min at 9 weeks of age. The same rat was tested in light/dark transition test, open field test, and Morris water maze test at 10–13 weeks of age. Rats were placed in the behavioral testing room at least 1 h before the start of tests.

Light/dark transition test

The light/dark box with grid floor (MELQUEST, Toyama, Japan) was used in this test. The apparatus consisted of two transparent compartments (45 × 27 × 26 cm) divided by a black guillotine door, and it had black and transparent lids. Inside of one compartment was covered with black walls and floor plates. Another floor was covered with a white floor plate. The light intensity of the center of the light compartment was 200–201 lux. Each rat was placed in the dark compartment of the box with the guillotine door closed. Immediately after opening the door, the behavior of each rat was recorded for 5 min with an animal movement analysis system with infrared sensors (SCANET MV-40, MELQUEST). The time spent in the light compartment, the number of transitions

between light and dark compartments, and the latency to enter the light compartment for the first time were analyzed.

Open field test

The gray square open field apparatus (70 × 70 × 40 cm, MUROMACHI Kikai, Tokyo, Japan) was used in this test. The apparatus was illuminated by indirect lighting, and the light intensity of the center of the field was 30 lux. Each rat was placed at the corner of the field, and the behavior of each rat was recorded for 10 min with ANY-maze Video Tracking System (Stoelting, Wood Dale, IL, USA). The distance traveled was analyzed.

Morris water maze test

The gray circle water pool apparatus (1.5 m in diameter, MUROMACHI Kikai) with the water temperature at 23°C–25°C was illuminated by indirect lighting. The light intensity of the center of the pool was 21–24 lux. Visual cues that surrounded the pool were the same during 4 training days and 1 probe test day. A transparent platform (12 cm in diameter, MUROMACHI Kikai) was located at the same position in the target quadrant (E) and hidden 2 cm below the water surface during training days. Each training day had four trials, and the time interval between each trial was more than an hour. The first trial of the next day was started more than 24 h after the first trial of the previous day. For learning the location of the platform, rats swam until they reached and stayed on it for 5 s. If rats couldn't reach the platform within 60 s, an experimenter guided rats to the platform, and rats were allowed to stay on the platform for 30 s. The probe test was performed >24 h after the final trial of the 4th training day. Rats swam in the pool without the platform for 60 s. The behavior of each rat was recorded with ANY-maze Video Tracking System. The escape distance during training days and the percent of time spent in each quadrant in the probe test were analyzed. Three problematic trial data (one trial for each rat) caused by the tracking error were excluded.

Brain morphometry by MRI

TcHSA21rats with >80% GFP-positive rates in PB-FCM and Eu littermates at ~4 months old were used for the *ex vivo* MRI analysis (n = 9 per group). Rats were perfused with PBS and then 4% PFA. Heads were post-fixed in 4% PFA at 4°C for 1 week and then kept in PBS for 3 days. We stored heads in Fomblin (Fomblin Profludropolyether, Ausimont, Thorofare, NJ, USA) to prevent dehydration during imaging in an 11.7 Tesla scanner (vertical bore, Bruker Biospin, Billerica, MA). 3D T2-weighted images were acquired with the resolution = 0.08 mm × 0.08 mm × 0.08 mm. For analysis, *ex vivo* images were first aligned to the template image with automated image registration software (Diffeomap) and adjusted to an isotropic resolution of 0.125 mm × 0.125 mm × 0.25mm. We quantitatively measured volume from different brain structures by combining automated and manual editing of images in ROIEditor.

Craniofacial morphology by micro-CT

High-resolution μCT images with a voxel size of 0.0300 mm were acquired by the Center for Quantitative X-Ray Imaging at the Pennsylvania State University with the HD-600 OMNI-X high-resolution X-ray computed tomography system (BioImaging Research). We used a minimum threshold of 70–100 mg/cm^3 partial density HA (based on HA phantoms imaged with specimens) to reconstruct isosurfaces in Avizo Lite 9.7 (Visualization Sciences Group). Micro-CT images of the heads of TcHSA21rats with >80% GFP-positive rates in PB-FCM (n = 7) and Eu (n = 10) littermates at ~4 months old were analyzed morphometrically. We collected 3D coordinates of 40 biologically relevant landmarks from the isosurfaces to use in analyses. Specimens were digitized three times, and intra-observer measurement error was minimized by averaging coordinates of the three trials (maximum accepted error in landmark placement = 0.05 mm). We used Euclidean distance matrix analysis (EDMA) to statistically evaluate skull shape differences by hypothesis test and confidence interval estimation.[36] EDMA is a 3D morphometric technique invariant to the transformation group, including translation, rotation, and reflection.[37,38] Briefly, the original 3D coordinates of landmark locations are rewritten and analyzed as a matrix of all unique linear distances among landmarks called the form matrix (FM). An average FM is estimated for each sample.[38] The difference between samples is evaluated by estimating ratios of like linear distances with sample-specific average FMs. The resulting matrix of ratios, the form difference matrix (FDM), is a collection of relative differences among landmarks used to define the forms. A non-parametric bootstrap procedure (100,000 resamples) is used to obtain confidence intervals for elements (each corresponding to a linear distance) of the FDM[36] that reveals the localized effects of HSA21 on the skull. We also include a non-parametric bootstrap assessment of the null hypothesis that the mean forms of two samples are the same.[36] We measure form differences of the facial skeleton, the cranial base, and the cranial vault by using landmarks specific to those regions and the software WinEDMA.

We used generalized Procrustes analysis (GPA) to extract shape coordinates from the landmarks measured on the entire craniofacial skeleton. GPA calculates shape coordinates from the original landmark dataset by translating, scaling, and rotating the data and subsequently yielding Procrustes shape coordinates. A measure of overall size, called Centroid size (CS), is calculated as the square root of the sum of squared Euclidean distances from a set of landmarks to their centroid.[39,40] Using the Procrustes coordinates, we explored patterns of shape variation in the dataset by using principal-component analyses (PCAs). PCA is based on an eigenvalue decomposition of a covariance matrix, transforming Procrustes shape coordinates into scores along principal components.[40] PCA was performed with all forty cranial landmarks in our dataset. All other morphometric and statistical analyses, including the construction of the wireframe diagrams, were performed in MorphoJ (Klingenberg lab) and R programming software (version 4.0.1).

Immunostaining

After MRI scan, brains of TcHSA21rat and Eu (n = 4 per group) were removed, fixed in 4% PFA overnight at 4°C, and transferred to 30% sucrose for 48 h. 30 or 40 μm sagittal cryosections were collected onto glass slides. Dry slides were post-fixed in 4% PFA and treated with 0.5% Triton in PBS. Parasagittal sections were immunostained with anti-calbindin (Cell Signaling, #13176) and DAPI.

CHD analysis by wet dissection

Embryonic day 20.5 (E20.5)–E22.5 rat fetuses were removed and sacrificed, and hearts were flushed with PBS via the umbilical vein and then fixed in 4% PFA. The hearts were examined for cardiovascular anomalies under a dissecting microscope.

Statistical analysis

For each experiment, we stated statistical information, including the exact sample size, statistical tests, and the exact p values in each figure or its legend. Unless otherwise noted, data were expressed as mean ± SEM (the standard error of the mean), and p value < 0.05 was considered as statistically significant. Statistical programs including Microsoft Excel (Microsoft, USA), SPSS Statistics 25 (IBM, USA), GraphPad Prism (GraphPad Software, USA), and R programming software (version 4.0.1) were used. A consolidated statistical table for each figure was provided in Table S10.

Results

The generation and WGS of TcHSA21rat

The hybrid A9 cells containing a copy of HSA21 were described previously.[41] Because DT40 cells have a high frequency of homologous recombination, the HSA21 was moved from A9 into DT40 cells through microcell-mediated chromosome transfer (MMCT).[31,32] In hybrid DT40 cells, the HSA21 was modified with a loxP site at the peri-centromeric gene-free locus, "NC_000021.9" (from 13,021,348 bp to 13,028,858 bp), to form the "HSA21-loxP" chromosome.[31] In this study, the HSA21-loxP chromosome was then transferred from DT40 into HPRT-deficient Chinese hamster ovary (CHO) cells by MMCT (Figure 1A). To monitor the HSA21 stability in cells, we inserted CAG promoter-driven EGFP into the loxP site of HSA21-loxP to generate the "HSA21-EGFP" chromosome through Cre-loxP recombination (Figure S1A). Recombinant clones were selected with HAT, and six out of six HAT-resistant clones were positive by PCR with Cre-loxP recombination-specific primers. The recombination process was confirmed by fluorescence *in situ* hybridization (FISH) (Figures S1B and S1C).

HSA21-EGFP was then transferred from CHO cells into "BLK2i-1" rat embryonic stem (ES) cells (RGD: 10054010) via MMCT, producing two rat ES clones with a freely segregating HSA21-EGFP chromosome based on FISH analysis (Figure 1B). We microinjected cells from the rat ES clone with a major karyotype of 43,XY,+HSA21-EGFP into the blastocoel cavity of host Crlj:WI blastocysts (Charles River Laboratories Japan, Kanagawa, Japan) to produce chimeras. Sixty-five offspring were produced from 125 rat ES-injected blastocysts, and 53 out of 65 offspring (82%) were chimeric (Table S2). Among 19 male chimeras, one rat had a GFP-positive seminiferous tubule (Figure S1D). Round spermatids of the GFP-positive male chimeric rat were injected into rat ooplasm with round spermatid injection (ROSI), and five of 13 offspring were GFP-positive (Table S3). We then crossed three GFP-positive females with Crlj:WI (Wistar) males to establish the transchromosomic rat model of DS named "TcHSA21rat." Pups could be recognized with a UV flashlight (Figure 1C). The supernumerary HSA21 was visualized in lymphocytes by FISH (Figure 1D).

Although the annotation of HSA21p in GRCh38.p12 shows 17 protein-coding genes (PCGs), 15 of them are not well annotated (Table S4A) and are currently either considered as HSA21q paralogs or genome assembly errors.[15,42] *BAGE2* and *TPTE* may be the only two bona fide PCGs on HSA21p. *BAGE2* has no reported mouse or rat orthologs, while *TPTE* has an annotated mouse ortholog on MMU10 but does not have any rat ortholog. Three-way comparison of HSA21q orthologous relationships based on genome assemblies of human (GRCh38.p12), rat (Rnor_6.0), and mouse (GRCm38.p6) document evolution between these species (Figure 1E). After excluding 49 keratin-associated protein genes (*KRTAP*s), 158 out of 164 HSA21q PCGs have orthologs in both rat and mouse; the exceptions are *POTED*, *TCP10L*, *AP000295.1*, *AP000311.1*, *SMIM34A*, and *H2BFS*. The "*LIPI-ZBTB21*" orthologous segments are found on RNO11 and MMU16, while "*UMODL1-PRMT2*" orthologous segments are on RNO20 but are divided in mice between MMU17 and MMU10. The PCG arrangement in orthologous segments is the same among three species except for the rat *Hmgn1* (Table S4B); this may be an annotation issue of the rat genome. WGS analysis showed two deletions in the HSA21-EGFP in TcHSA21rat (Figure 1F and Table S4C). Deletion 1 (17,843,345–23,995,878) contains three PCGs, and the same deletion occurs in TcMAC21.[15] Deletion 2 (28,195,594–30,325,968) is specific to the TcHSA21rat and contains three *KRTAPs* and ten non-*KRTAP* PCGs. Together, HSA21-EGFP of TcHSA21rat contains 214 out of 230 (93%) HSA21 PCGs and lacks 13 non-*KRTAP* PCGs (annotated in Table S4D).

The presence of HSA21 causes global transcriptional imbalance in TcHSA21rat

Forebrain transcripts from three pairs of TcHSA21rat and euploid (Eu) littermates at postnatal day (P)1 were analyzed by RNA-seq (Table S5A). We reported our results in FPKM (fragments per kilobase of transcript per million mapped reads). Because TcHSA21rat contained one copy of HSA21, we used FPKM = 0.5 as the cutoff to determine whether an HSA21 gene was expressed or not. Two PCGs mapped to HSA21p (the short arm), *BAGE2* (FPKM = 7.9) and *TPTE* (FPKM = 5.0), were expressed (Table S5B). Among 213 HSA21q PCGs, none of 49 *KRTAP*s were expressed (<0.5 FPKM) as expected, and 76 of 164 (46.3%) non-*KRTAP* PCGs had >5 FPKM (Figures 2A and 2B). In contrast, nine of 601 (1.5%) HSA21 non-PCGs had >5 FPKM. Neither HSA21 PCGs in deleted regions nor five PCGs with no mouse or rat orthologs (*TCP10L*, *AP000295.1*, *AP000311.1*, *SMIM34A*, and *H2BFS*) were expressed in the P1 forebrain.

There were 120 HSA21 orthologs with FPKM ≥ 1 in the forebrain of P1 Eu rats, and 69 of them were expressed at medium or high levels (FPKM ≥ 10, Table S5C). To analyze HSA21 dosage changes, we utilized two FPKM cutoffs (FPKM ≥ 1 (Table S5D) and FPKM ≥ 10 (Table S5E). We determined that the expression of rat orthologs of HSA21 was substantially the same in euploid and TcHSA21rat (Figure 2C): of 69 HSA21 rat orthologs with FPKM ≥ 10, 67 were expressed at 80%–120% of Eu levels in TcHSA21rat, two (*Olig1* and *Olig2*) had reduced expression

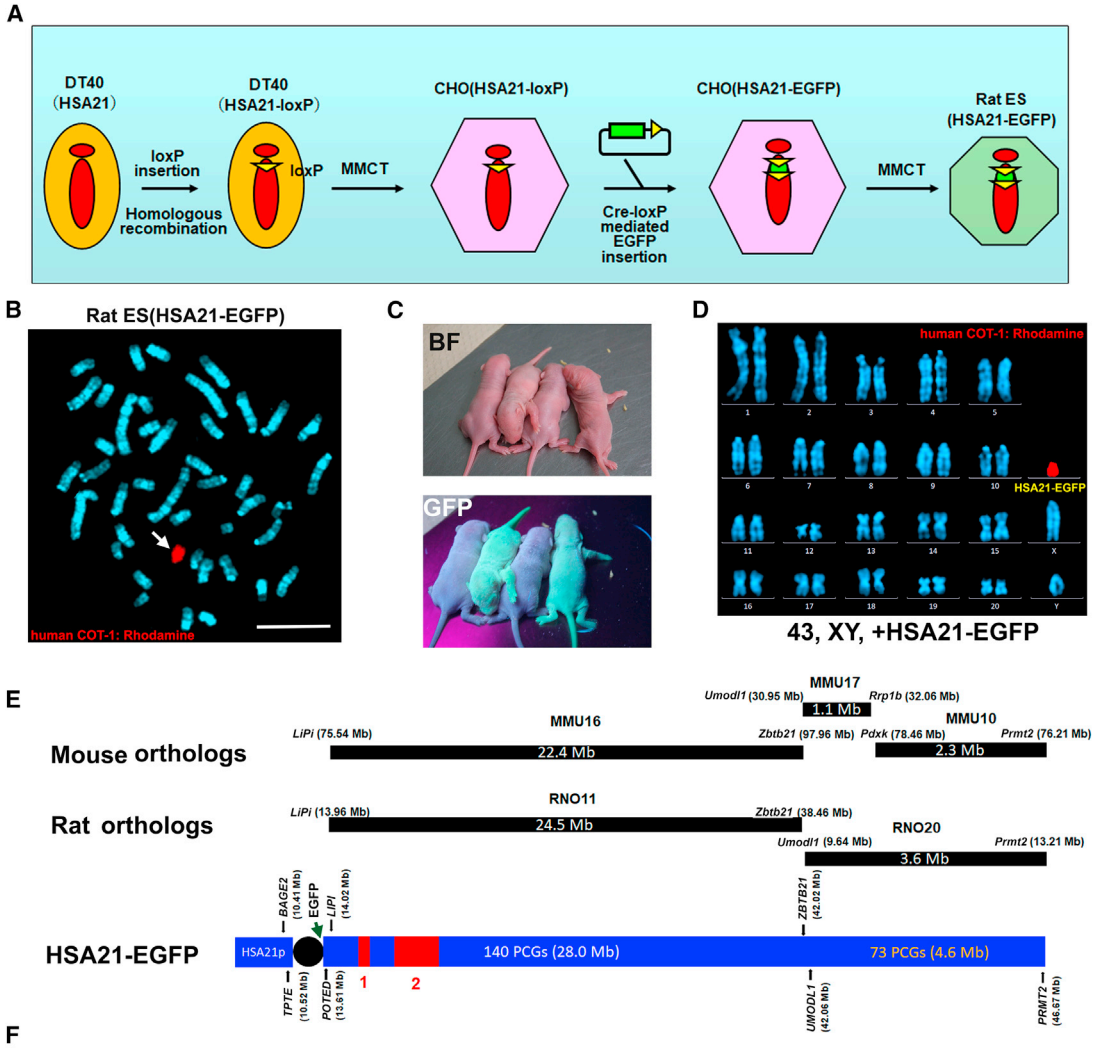

F

Deleted.region	Start	End	Deleted size (bp)	% of HSA21	% of HSA21q	PCG	non-PCG
Deletion 1	17,843,345	23,995,878	6,152,534	13.2%	18.3%	3 (*CHODL, TMPRSS15, NCAM2*)	56
Deletion 2	28,195,594	30,325,968	2,130,375	4.6%	6.3%	13 (*N6AMT1, LTN1, RWDD2B, USP16, CCT8, MAP3K7CL, BACH1, GRIK1, CLDN17, CLDN8, KRTAP24-1, KRTAP25-1, KRTAP26-1*)	24
Total			8,282,909	17.7%	24.6%	16	80

Figure 1. Generation of TcHSA21rat and WGS of the HSA21

(A) Schematic diagram of HSA21-EGFP construction and MMCT.

(B) FISH of rat ES (HSA21-EGFP) cells. Digoxigenin (Rhodamine)-labeled human COT-1 DNA as the FISH probe for HSA21 and DNA counterstained with DAPI. Scale bar, 10 μm.

(C) TcHSA21rat and euploid (Eu) pups visualized by GFP flashlight. BF, bright field.

(D) Karyotype of TcHSA21rat lymphocytes. Digoxigenin (Rhodamine)-labeled human COT-1 DNA as the FISH probe for HSA21-EGFP.

(E) The orthologous relationships between HSA21, rat chromosomes, and mouse chromosomes. The HSA21-EGFP cartoon is normalized to PCG numbers. The positions and sizes of the two deletions detected by WGS are shown in red.

(F) Summary of positions and genetic contents of the deletions in HSA21-EGFP.

(<0.8-fold) and none showed increased expression (>1.2 fold). To quantify total HSA21 overexpression levels in TcHSA21rat, the FPKM sum of an HSA21 PCG and its rat ortholog were compared between Eu and TcHSA21rat. When using FPKM ≥ 10 as the cutoff, we found that 25% were in the low overexpression range (<1.3-fold increased over Eu), 43.8% in the expected range (1.3–1.7-fold), and 31.3% in the highly overexpressed range (>1.7-fold, Figure 2C). When using FPKM ≥ 1 as the cutoff, 23.6% were in the low overexpression range, 31.8% in the expected range, and 44.5% in the highly overexpressed range (Figure S2A).

Disruption of global transcription has been reported in people with DS and DS mouse models.[15,43–45] To analyze the effect of trisomy on global gene expression, we compared transcript levels of all rat genes (both

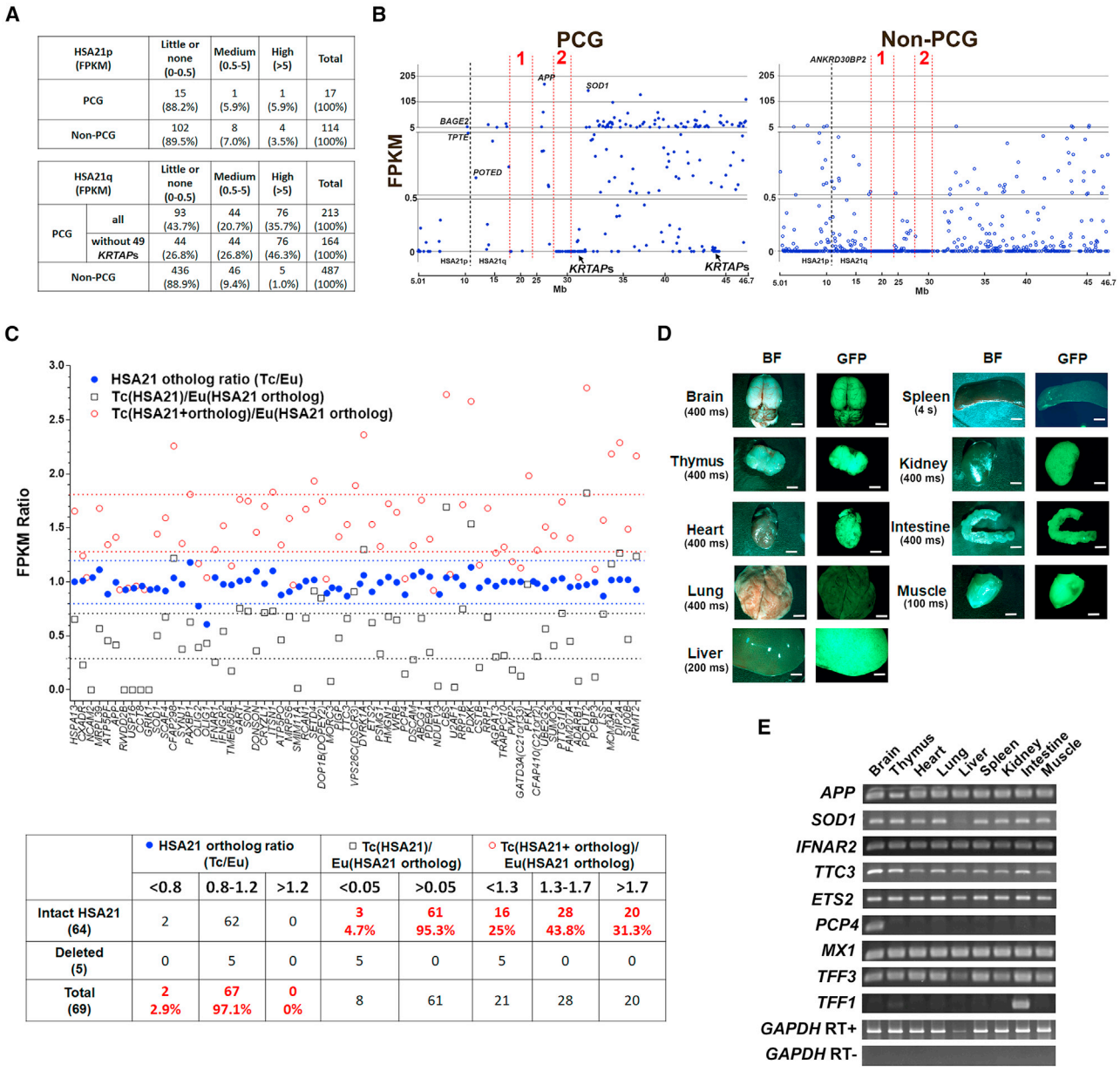

HSA21p (FPKM)	Little or none (0-0.5)	Medium (0.5-5)	High (>5)	Total
PCG	15 (88.2%)	1 (5.9%)	1 (5.9%)	17 (100%)
Non-PCG	102 (89.5%)	8 (7.0%)	4 (3.5%)	114 (100%)

HSA21q (FPKM)		Little or none (0-0.5)	Medium (0.5-5)	High (>5)	Total
PCG	all	93 (43.7%)	44 (20.7%)	76 (35.7%)	213 (100%)
	without 49 *KRTAPs*	44 (26.8%)	44 (26.8%)	76 (46.3%)	164 (100%)
Non-PCG		436 (88.9%)	46 (9.4%)	5 (1.0%)	487 (100%)

	HSA21 ortholog ratio (Tc/Eu)			Tc(HSA21)/ Eu(HSA21 ortholog)		Tc(HSA21+ ortholog)/ Eu(HSA21 ortholog)		
	<0.8	0.8-1.2	>1.2	<0.05	>0.05	<1.3	1.3-1.7	>1.7
Intact HSA21 (64)	2	62	0	3 4.7%	61 95.3%	16 25%	28 43.8%	20 31.3%
Deleted (5)	0	5	0	5	0	5	0	0
Total (69)	2 2.9%	67 97.1%	0 0%	8	61	21	28	20

Figure 2. The presence of HSA21 causes global transcriptional imbalance in TcHSA21rat

(A–C) Forebrains of P1 male Eu and TcHSA21rat littermates analyzed by RNA-seq (n = 3 per group). (A and B) Transcription levels of HSA21 PCGs and non-PCGs in P1 forebrain of TcHSA21rat analyzed by RNA-seq. (C) The comparisons of HSA21 PCGs and rat orthologs expression between TcHSA21rat and Eu among 69 HSA21 rat orthologs whose FPKM ≥ 10 in Eu. Three FPKM ratios are compared: Tc(HSA21)/Eu(HSA21 ortholog), the FPKM ratio of a HSA21 PCG in TcHSA21rat to its rat ortholog in Eu; HSA21 orthologs ratio (Tc/Eu), the FPKM ratio of a HSA21 rat ortholog in TcHSA21rat to that in Eu; and Tc(HSA21+orthologs)/Eu(HSA21 orthologs), the FPKM ratio of total expression (sum of an HSA21 PCG and its rat ortholog) in TcHSA21rat to that in Eu. The PCGs in deletions 1 and 2 are indicated in red lines. Tc, TcHSA21rat.

(D) TcHSA21rat organs visualized by GFP-UV light. The exposure time is shown, and scale bar, 5 mm. BF, bright field.

(E) RT-PCR analysis of nine TcHSA21rat organs using nine HSA21-specific primers. Primer information is available in Table S5F.

non-coding and coding) between Eu and TcHSA21rat. More than 900 of 13,473 rat genes with FPKM ≥ 1 in Eu were misregulated in trisomic rats (Table S6). Of these, 358 were downregulated (i.e., a rat gene in TcHSA21rat expressing less than 80% of Eu level) and 570 were upregulated (i.e., a rat gene in TcHSA21rat expressing more than 120% of Eu level). Human-specific RT-PCR for nine genes in nine organs showed that HSA21 genes had tissue-specific expression, e.g., the brain-specific transcript of PCP4 was detected only in brain and TFF1, expressed normally in intestine, was only observed in TcHSA21rat intestine (Figures 2D and 2E).

Together, these results indicate that in addition to altering HSA21 dosage, the presence of HSA21 causes global transcriptional imbalance in TcHSA21rat.

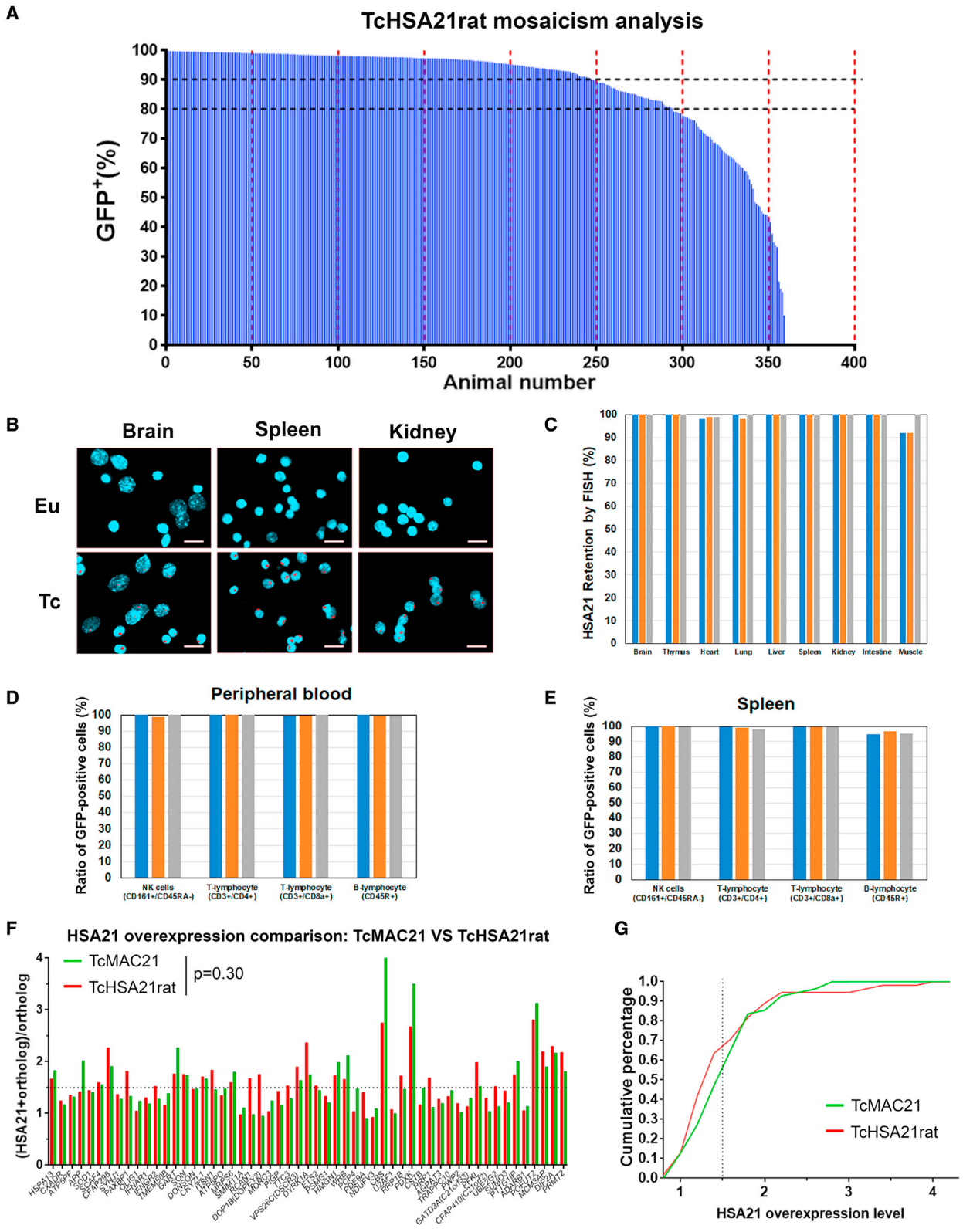

Figure 3. Mosaicism analysis of TcHSA21rat

(A) Mosaicism analysis of peripheral blood cells from 361 TcHSA21rats using FCM.

(B) Representative FISH images of isolated cells from Eu and TcHSA21rat tissues using Digoxigenin (Rhodamine)-labeled human COT-1 DNA as the HSA21 probe. Scale bar, 20 μm.

(C) Summary of FISH of various TcHSA21rat tissues. Different rats are shown by different one-color bars, and n = 3.

(D) FCM of NK cells and lymphocytes from PB (n = 3).

(E) FCM of NK cells and lymphocytes from spleen (n = 3).

(legend continued on next page)

The analysis of HSA21 mosaicism in TcHSA21rat

The transchromosomic mouse TcMAC21 shows stable transmission and retention of a hybrid chromosome containing HSA21q engineered with mouse centromere and telomere.[15] However, transchromosomic mice carrying human chromosomes or human artificial chromosomes (HACs) without mouse centromeres show high frequencies of mosaicism.[46–48] Retention rates of the foreign chromosome are lower in highly proliferative tissues, such as blood and spleen, than in slowly proliferative tissues, such as brain. Constitutive EGFP expression from HSA21-EGFP allows us to use FCM as a high-throughput tool to analyze HSA21 mosaicism in transchromosomic rodents. FCM of peripheral blood (PB) from 361 TcHSA21rats at 1 month old or older showed 69.3% of TcHSA21rats with >90% GFP-positive rates and 81.4% of TcHSA21rats with >80% GFP-positive rates (Figure 3A and Table S7A).

FISH of various tissues (brain, thymus, heart, lung, liver, spleen, kidney, small intestine, and skeletal muscle) from three TcHSA21rats with >90% GFP-positive rates in PB showed 92%–100% HSA21 retention rates (Figures 3B and 3C). FCM of NK cells ($CD161^+/CD45RA^-$), T-lymphocytes ($CD3^+/CD4^+$ or $CD3^+/CD8a^+$), and B-lymphocytes ($CD45R^+$) from the same rats showed >95% GFP-positive rates (Figures 3D and 3E). Correlation analysis showed that HSA21 retention rates in PB measured by FISH were strongly correlated with GFP-positive rates measured by FCM ($R^2 = 0.9882$, Figure S2B).

As TcMAC21 is not mosaic and contains almost the same HSA21 as TcHSA21rat, we compared HSA21 overexpression levels between TcHSA21rat and TcMAC21 on the basis of RNA-seq data of P1 forebrain from three pairs of Eu and TcHSA21rat littermates and two pairs of Eu and TcMAC21 littermates. Fifty-six HSA21 PCGs that were intact in both species and had FPKM $\geq$ 10 orthologs (Table S7B). The average overexpression (Tc/Eu ratio) of each HSA21 PCG from TcMAC21 and TcHSA21rat was measured and then compared as a whole via Wilcoxon matched-pairs signed-rank test (Mann-Whitney-Wilcoxon tests, $p = 0.3$, Figure 3F) and cumulative frequency distribution (Figure 3G), indicating that HSA21 overexpression patterns were similar between the two DS models.

TcHSA21rat shows altered cognitive and behavioral phenotypes

At about 3 months of age, Eu and TcHSA21rat (>80% GFP-positive rates in PB, n = 15 per group) males were assessed in the light/dark transition (LDT) test, the open field (OF) test, and the Morris water maze (MWM) test (Figure 4A). The LDT test, a widely used test to assess anxiety-like behavior in rodents,[49,50] showed that both the time spent in the light compartment and the number of transitions between light and dark compartments were significantly decreased in TcHSA21rat compared with Eu ($p < 0.05$, unpaired t test, Figures 4B and 4C). TcHSA21rat also had increased latency to enter the light compartment ($p = 0.06$, Mann-Whitney U test as Eu group did not pass normality test because of two outliers (ROUT method [robust regression followed by outlier identification] [Q = 1%], Figure 4D; $p = 0.008$, unpaired t test if those two outliers were excluded, Table S10). In the OF test that has been widely used to evaluate novelty-induced exploratory activity in mice and rats,[15,51,52] TcHSA21rat showed a significant increase in the total distance traveled compared with Eu ($p = 0.001$, unpaired t test, Figure 4E).

The MWM paradigm consisted of 4 days of acquisition trials and a probe trial conducted 24 h after the last acquisition trial was used to assess spatial learning and memory. As TcHSA21rat swam faster than Eu in acquisition trials ($p = 0.01$, two-way repeated-measures [RM] ANOVA, Figure 4F), the performance in acquisition trials was reported as escape distance rather than latency. Training improved escape distance in both groups, but the improvement was significantly slower in TcHSA21rat than in Eu ($p = 0.01$, two-way RM ANOVA, Figure 4G). In probe trials, TcHSA21rat spent substantially less time than Eu in the target quadrant ($p < 0.05$, two-way ANOVA and Sidak's multiple comparisons test, Figures 4H and 4I). Unlike Eu rats that had a strong preference for the target quadrant ($p = 0.001$, target versus adjacent, two-way ANOVA and Tukey's multiple comparisons test), TcHSA21rat had no preference for the target quadrant ($p = 0.98$, target versus adjacent, two-way ANOVA and Tukey's multiple comparisons test). Together, the various behavior tests indicate that TcHSA21rat has higher anxiety, locomotor hyperactivity, and learning and memory deficits.

TcHSA21rat has distinct alterations in brain morphology and cerebellar foliation

Brain morphometry of Eu and TcHSA21rat males at about 4 months of age (>80% GFP-positive rates in PB, n = 9 per group) was analyzed with T2-weighted MRI. Total brain volume of TcHSA21rat was significantly smaller than Eu (2266 ± 80 mm^3 versus 2379 ± 73 mm^3, $p = 0.009$, unpaired t test, Figure 5A). Among major brain structures, cerebellums ($p < 0.0001$, unpaired t test) of TcHSA21rat were significantly smaller than those of Eu. The average cerebellar volume of TcHSA21rat was ~86% of Eu. When normalized to the total brain, the percentage volume of cerebellum was disproportionately decreased in TcHSA21rat ($p < 0.0001$, 14.1% in TcHSA21rat versus 15.7% in Eu, unpaired t test, Figure 5B). In contrast, the percentage volume

(F and G) The HSA21 overexpression pattern comparison between TcHSA21rat and TcMAC21 based on RNA-seq of P1 forebrain (Eu and TcHSA21rat littermates, n = 3 per group; Eu and TcMAC21 littermates, n = 2 per group). 55 HSA21 PCGs are compared on the basis of two criteria: (1) HSA21 PCGs are intact in both TcMAC21 and TcHSA21rat and (2) FPKM of HSA21 orthologs $\geq$ 10. (F) Overexpression pattern of individual PCG from TcHSA21rat and TcMAC21, and the differences are analyzed by Mann-Whitney test (Wilcoxon matched-pairs signed-rank test). (G) Cumulative distribution of overexpression levels.

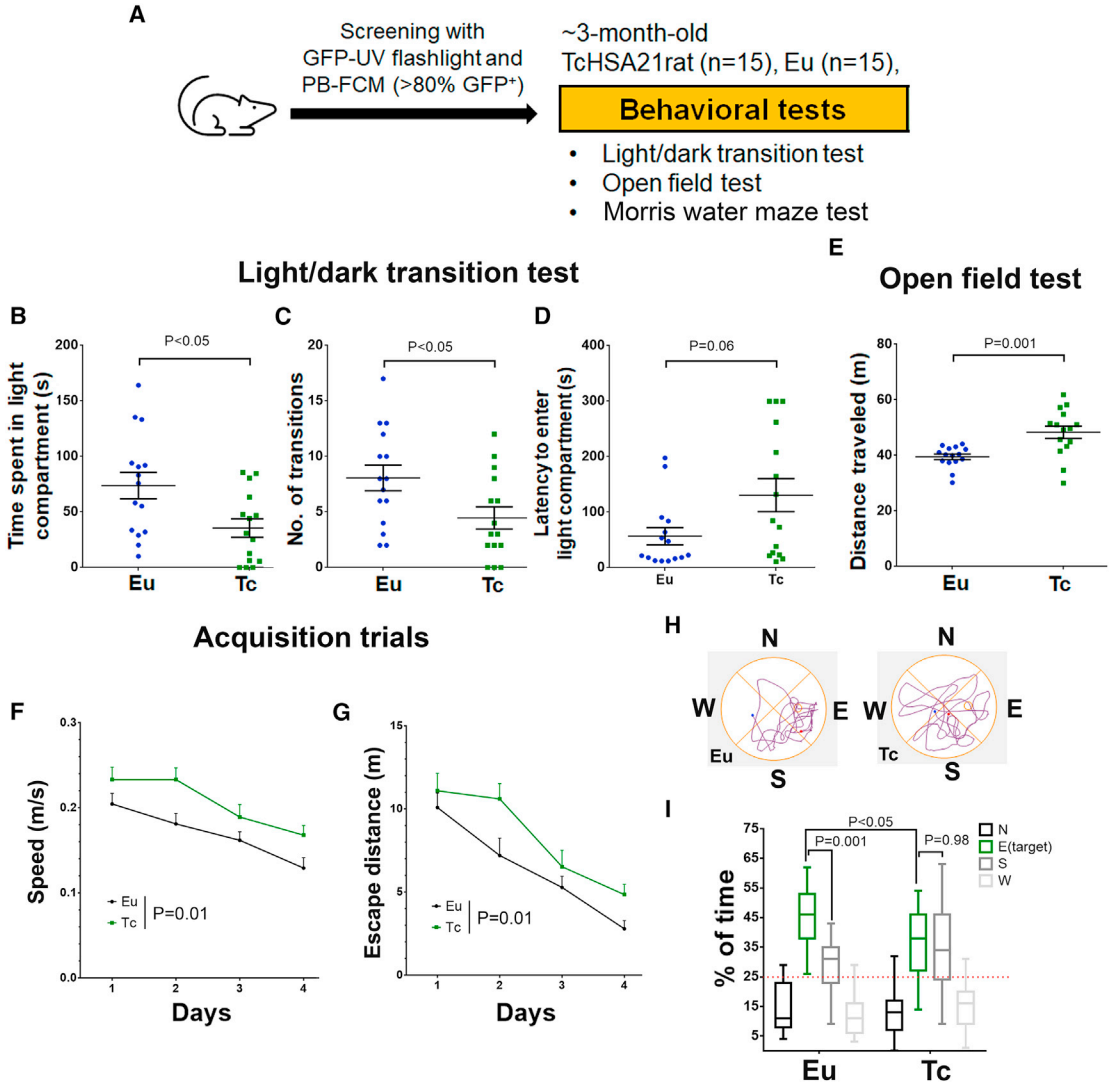

Figure 4. TcHSA21rat shows higher anxiety, hyperactivity, and learning and memory deficits

(A) The experimental design for behavioral tests (n = 15 per group).

(B–D) Light/dark transition test: (B) the time spent in the light compartment; (C) the number of transitions between light and dark compartments; (D) The latency time to enter the light compartment. Data are analyzed by unpaired Student's t test (B and C) and by Mann-Whitney U test (D).

(E) Open field test. The total distance traveled is compared with unpaired Student's t test.

(F–I) Morris water maze test: (F and G) Swimming speed and escape distance in acquisition trials, and data are analyzed by repeated-measures two-way ANOVA; (H) representative tracking plots of the probe trials; (I) probe trials, data are analyzed by two-way ANOVA and Sidak's post hoc for comparing the percentage of time spent in each quadrant between Eu and TcHSA21rat and Tukey's post hoc for analyzing whether animals prefer the target quadrant, and the whiskers show 2.5–97.5 percentiles. All data are expressed as mean with SEM. Eu, Euploid rat; Tc, TcHSA21rat.

of midbrain regions, such as thalamus and superior colliculus, were increased in TcHSA21rat.

Due to larger brain size, we found better visualization of cerebellar vermian lobules (midsagittal section) in rat brain MRI (Figure 5C) than mouse brain MRI.[15] TcHSA21rat showed significantly fewer sublobules than Eu on the basis of both MRI (Figure 5C) and histology analyses (Figures 5D and 5E). This phenotype was consistently observed in all nine TcHSA21rats analyzed (Figure S3). Together, these data show that TcHSA21rat not only recapitulates well-characterized DS brain phenotypes (i.e., smaller brain and disproportionately small cerebellum) but also has reduced cerebellar foliation, a feature not captured in DS mouse models.

TcHSA21rat shows anomalies in craniofacial morphology, heart development, husbandry, and stature

Micro-computed tomography (micro-CT) images of the heads of ~4 months old TcHSA21rat (n = 7) and Eu (n = 10) littermates were analyzed morphometrically with 40 3D cranial landmarks (lms) (Figure 6A, Figure S4, and Table S8). EDMA[36] revealed statistically significant differences between TcHSA21rat and Eu for subsets of measures

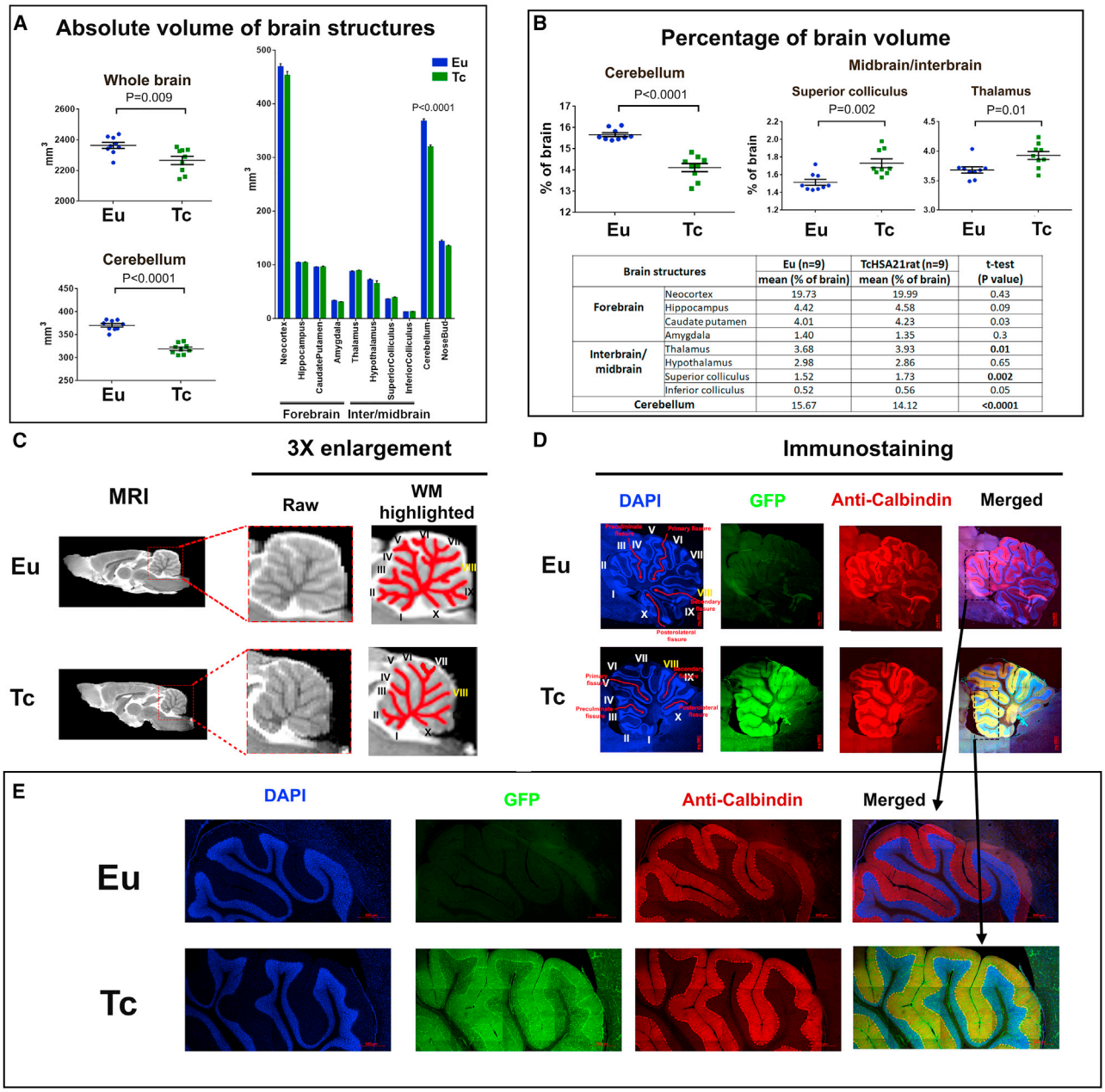

Figure 5. TcHSA21rat has distinct alterations in brain morphometry and cerebellar foliation

(A) Statistical analysis of absolute volumes of whole brain and its subregions based on T2-weighted MRI (n = 9 per group). Data are analyzed by unpaired Student's t test.

(B) Statistical analysis of percentage volume of brain subregions. Data are analyzed by unpaired Student's t test.

(C) Representative T2-weighted MRI of Eu and TcHSA21rat brains. Both raw cerebellum MRI and white matter (WM) highlighted MRI are shown.

(D and E) Immunostaining of parasagittal brain sections with anti-calbindin antibody (red) and DAPI (blue). Eu, Euploid rat; Tc, TcHSA21rat.

that defined the cranial base, cranial vault, and facial skeleton ($p \leq 0.025$, non-parametric bootstrap, Table S10). The TcHSA21rat craniofacial skeleton is generally smaller than Eu. 90% bootstrap confidence intervals[38] of linear distances between landmarks showed localized effects of HSA21 concentrated on the facial skeleton, with additional, more subtle effects on the cranial vault (Figure 6A). In agreement with the EDMA, generalized-Procrustes-based PCA of craniofacial shape variables revealed the facial skeleton of TcHSA21rat to be retracted and the posterior cranial vault to be "rounded" relative to Eu (Figures 6B and 6C). Principal component axis 1 (PC 1) explained 45.3% of the total variance in the sample and captured between-group differences between TcHSA21rat and Eu (Figure 6B). TcHSA21rat occupied the positive end on PC 1, indicating an antero-posteriorly

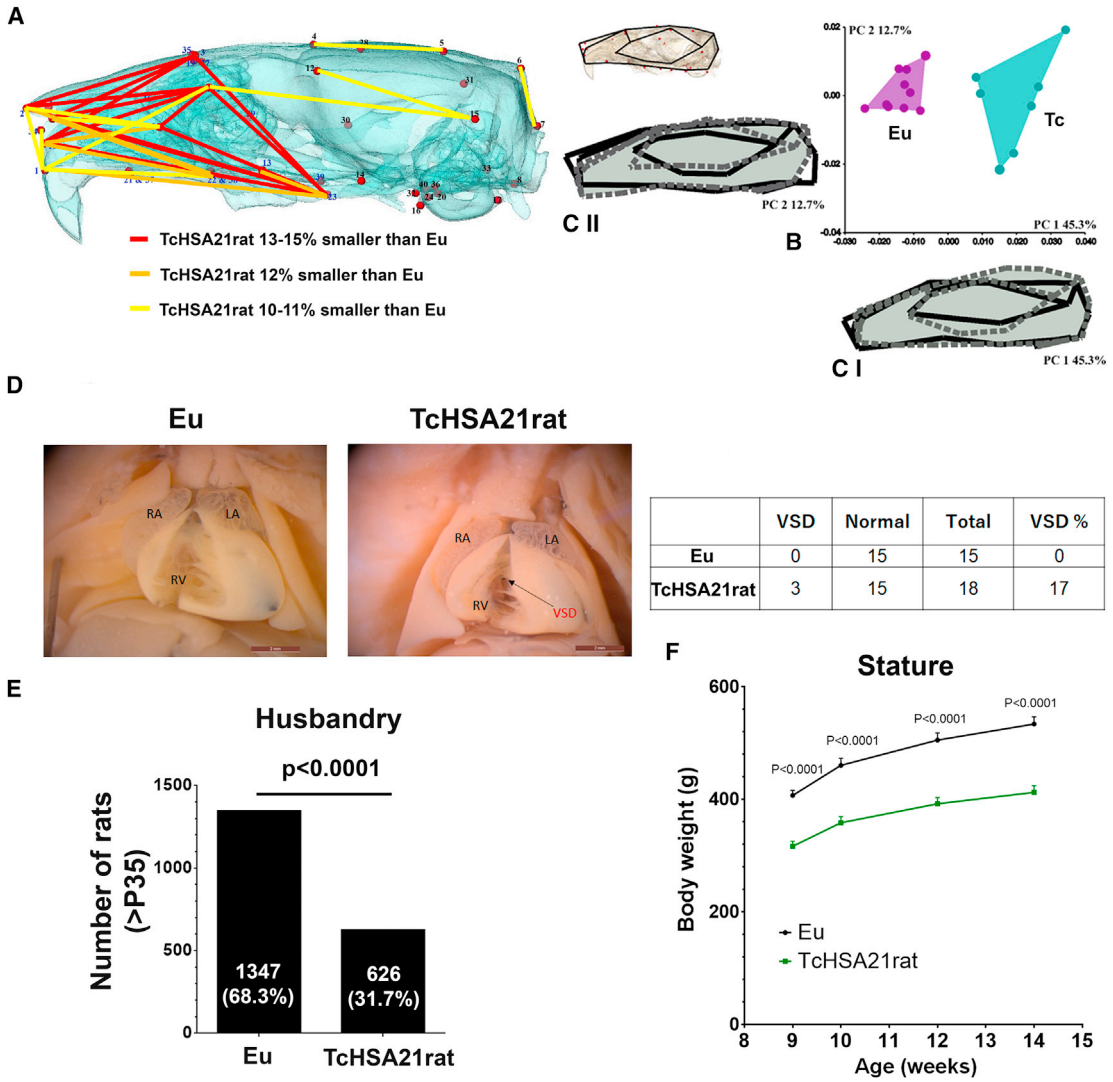

Figure 6. TcHSA21rat shows anomalies in craniofacial morphology, heart development, husbandry, and stature

(A–C) Craniofacial morphology analysis of Eu (n = 10) and TcHSA21rat (n = 7) in 4-month-old animals. (A) Statistically significant differences in cranial morphology between Eu and TcHSA21rat estimated by EDMA. The partially transparent bone segmented from HRμCT images is shown to better visualize the differences; the rostrum is at left and the occiput is at right. The linear distances pictured are limited to those that differed significantly by ≥10% (using $\alpha = 0.10$ confidence limits) and represent significantly smaller dimensions in TcHSA21rat. Different colored lines represent the percent differences. (B) PCA plot to show between-group differences (PC 1) and within-group variations (PC 2). (Ci) Shape change on the positive end of PC 1 is represented by the dashed and shaded wireframe diagram of the cranium. Positive scores show a retraction of the snout and superiorly raised posterior cranial vault. The solid black wireframe represents the negative end of PC 1 and shows an elongated overall cranial shape. (Cii) Shape changes on PC 2 are mainly related to the snout and inferior cranial base orientation. The dashed and shaded wireframe and the solid black wireframe represent the shape changes on the positive end and the negative end of PC 2, respectively.

(D) CHD analysis of Eu (n = 15) and TcHSA21rat (n = 18) at E20.5–E22.5 by wet dissection. Of 18 TcHSA21rat hearts, three hearts showed ventricular septal defect (VSD, arrow). LA, left atrium; RA, right atrium; RV, right ventricle.

(E) The offspring number of TcHSA21rat mothers from 263 litters. Only P35 or older offspring are counted. Data are analyzed by both the Chi-square test ($p < 0.0001$) and the binomial test ($p < 0.0001$).

(F) Body weight difference between TcHSA21rat and Eu males at 9, 10, 12, and 14 weeks old (n = 15 per group). Data are analyzed by unpaired Student's t test.

retracted face associated with a supero-inferiorly "raised" cranial vault (Figures 6A and 6Ci). PC 2 (12.7%) accounted for within-group variation, and TcHSA21rat showed more variation than Eu. Shape differences along this axis were mainly concentrated in the orientation of the snout and postero-inferior aspect of the neurocranium (Figure 6Cii).

The hearts of TcHSA21rats (n = 18) and Eu (n = 15) littermates were analyzed by wet dissection at E20.5–E22.5, showing that three (17%) TcHSA21rat hearts and none of Eu hearts had ventricular septal defect (VSD) (Figure 6D).

As no fertile TcHSA21rat males have been observed, TcHSA21rat is maintained through female transmission. The breeding record of 263 litters showed a trisomy

frequency of 32% among 1,973 offspring at age P35 or older ($p < 0.0001$, binomial test, Figure 6E), with an average litter size of 7.5. Comparison of trisomy frequency at E20.5–E22.5 and at P35 (Table S9) indicated a perinatal loss in TcHSA21rat. The mass of TcHSA21rat males measured from week 9 to week 14 was consistently lower than Eu counterparts, with an average weight reduction of ~20% ($p < 0.001$, unpaired t test, Figure 6F).

Discussion

We generated a transchromosomic rat model of DS, "TcHSA21rat," containing a freely segregating, EGFP-labeled HSA21 with 93% of HSA21 PCGs and exhibiting features analogous to those in people with DS. HSA21 genes are expressed and cause an imbalance in global gene expression in TcHSA21rat. Young adult TcHSA21rat displays learning and memory deficits and also exhibits robust DS brain phenotypes, including smaller brain volume, disproportionately small cerebellum, and reduced cerebellar foliation. TcHSA21rat has an altered craniofacial skeleton, higher CHD prevalence, male infertility, higher postnatal mortality, and smaller stature. Our study provides the initial validation of TcHSA21rat that could act as the "Pharma-preferred" model for DS research.

Rat versus mouse models for DS research

Rats lack the wealth of genetic stocks available for research in mice, although advances in both embryology and CRISPR have made the rat considerably more accessible as a genetic model. Rats possess several advantages for preclinical research compared to mice. The most obvious is size. Surgical interventions and assessments of anatomical changes are more accessible. A newborn rat is already 6–8 times the mass of a newborn mouse. Anatomical features are larger and, as shown here for cerebellum, may be more elaborated. Behavior testing for rats is more nuanced than for mice, which is a useful feature for DS research. Finally, rats are the traditional model for pharmaceutical development, and this wealth of experience may pay a dividend in translation of preclinical results to drug trials.

The cerebral cortex of lissencephalic species, including mice and rats, is smooth.[53] However, cerebellums of both mice and rats are foliated into five cardinal lobes. Rats show more complex cerebellar foliation than mice. Compared with Eu counterparts, the nearly identical trisomy causes significantly reduced foliation in TcHSA21rat but not in TcMAC21 (Figure S5). TcHSA21rat is the first DS animal model showing reduced cerebellar foliation. Moreover, the reductions in both the absolute and percentage volume in the TcHSA21rat cerebellum detected by MRI are more robust than observed in other aneuploid mouse models of DS (Ts65Dn,[54] Tc1,[55] and TcMAC21[15]). The larger cerebellar size facilitates assessment of cerebellar cortical changes in TcHSA21rat and, with attenuated foliation, should provide a useful model for understanding cerebellar hypoplasia and its role in DS cognitive phenotypes.

People with DS have smaller overall brain volume,[56] which is not well recapitulated in adult (>3 months old) aneuploid DS mouse models[15,54,55] but is readily observable in TcHSA21rat by MRI. As with mouse models, the changes in the rat comprise midface skeletal retrusion plus a reduced mandible, recapitulating changes in the DS craniofacial skeleton. As with mouse DS models, we see increased septal defects in TcHSA21rat but not the high level of congenital heart defects observed in people with DS. Twenty percent of babies with DS have complete AV canal (atrioventricular septal defect),[57] but like other rodent models of DS, this is not present in TcHSA21rat.

A major goal of DS research is to ameliorate the cognitive impact of trisomy. Both anxiety and attention deficit hyperactivity disorder (ADHD) are significantly more frequent in children with DS.[58–61] DS mouse models, Ts65Dn and Tc1, show hyperactivity but not anxiety-like behaviors.[14,62–64] Here, we demonstrate that in addition to learning and memory deficits, TcHSA21rat shows both anxiety-like behavior and hyperactivity.

Mosaicism and TcHSA21rat

About 90%–95% of people with DS are characterized as non-mosaic DS, while 2%–4% have segmental trisomy for a portion of HSA21 because of duplication or translocation and 2%–5% have mosaic DS.[65] There is no rigorous standard for declaring an individual to have mosaic DS. Although some laboratories use a more stringent criterion, typically the occurrence of trisomy 21 in 16 or more of 20 metaphases from peripheral blood cells is considered to be non-mosaic DS.[65] Individuals with mosaic DS generally have a milder clinical presentation than non-mosaic DS during the prenatal and perinatal period; it is not unusual for mosaic DS to be detected in older children or adults.[66,67] According to a population-based study by Devlin and Morrison,[68] only 37.5% of mosaic DS was detected by clinical examination, compared with a near 100% detection rate of non-mosaic DS.

Here, as HSA21 in both TcHSA21rat and TcMAC21 are marked by EGFP, we are able to determine mosaicism frequency in PB with high precision by using FCM. About 70% of TcHSA21rats have >90% GFP-positive rate in peripheral blood cells, while about 80% of TcHSA21rats meet the usual laboratory definition of non-mosaic DS (i.e., >80% trisomic karyotypes). The previous examination of TcMAC21 mice shows little mosaicism.[15] That observation is extended here by PB-FCM of 363 trisomic TcMAC21 mice, showing that ~95% of TcMAC21 mice are not mosaic with the GFP-positive rate of 80% as the cutoff (Figure S6). TcHSA21rat with a high percentage of trisomic PB showed similarly high HSA21 retention rates in different tissues. Through TcHSA21rat female transmission, the average litter size is 7.5, and 32% are GFP-positive when measured at P35. Therefore, the average number of non-mosaic TcHSA21rat per litter is 1.7 (90% GFP-positive rate in PB-FCM as cutoff)

or 2.0 (80% GFP-positive rate in PB-FCM as cutoff), similar to frequencies of some successful mouse DS models.

Future research

Human chromosomes are not mitotically stable in mouse cells and are stochastically lost over time.[32,46,47,69,70] Previous studies indicate that the loss rate per mitosis may vary from a few tenths of one percent to a few percent.[46,69,71] Prior analysis of mosaicism in hepatocytes from nine Tc1 transchromosomic mice suggests that the retention rates of HSA21 vary from 35%–75% in the liver, assuming similar efficiencies of RT-PCR amplification of human and mouse orthologs.[48] Similarly, transchromosomic mice containing an EGFP-labeled, HSA21-derived HAC (21HAC2) show <50% GFP-positive rates by PB-FCM (Figure S7). In contrast to mice, the rat shows greater tolerance to human centromeres. Elucidating reasons for this difference may facilitate the production of humanized mouse or rat models.

Reduced cerebellar foliation is a feature not captured in previous DS mouse models. It will be interesting to use neuroimaging to validate reduced foliation/gyration in the DS brain. High-resolution MRI capable of detecting alterations at microstructure (cellular) levels could enhance the MRI application to monitor disease progression in DS or neurological disorders. We recently used oscillating gradient diffusion MRI to detect subtle changes in different cerebellar layers of Ts65Dn that are not detectable in conventional MRI.[72] TcHSA21rat is a useful model for generating a rat cerebellar microstructure atlas for diffusion MRI over the course of development.

TcHSA21rat shows robust neurological phenotypes, replicating and extending observations in DS mouse models. Testing current candidate approaches for therapies targeting neurological phenotypes of DS (genes, peptides, or small molecules) will help prioritize clinical trials. In this regard, it will be interesting to study the TcHSA21rat regarding Alzheimer disease (AD). All people with trisomy 21 develop AD-like histopathology by the fourth decade in contrast to the general population, where AD is not generally diagnosed until the onset of behavioral symptoms. Attempts to ameliorate the onset of AD symptoms remain largely focused on eliminating amyloid plaques, and TcHSA21rat might support or refine these attempts.

Finally, in considering any model system, it is important to note that Down syndrome is a human condition. We recently reviewed the many caveats to the use of animal models to study this extremely complex genetic challenge to human development that affects every cell from (at least) conception onward.[9] In the case of rodent models, these include expected differences in stoichiometry of interactions between human and non-human orthologous proteins. As we note in that review, "The best animal models are tools for studying Down syndrome: they do not have Down syndrome."

Concluding remarks

TcHSA21rat meets the genetic criteria for a good DS model, including aneuploidy, minimal mosaicism, a large number of functionally trisomic HSA21 genes/orthologs, and no functionally trisomic or monosomic non-HSA21 genes/orthologs. With robust DS-related phenotypes, TcHSA21rat has the potential to accelerate preclinical studies and translation of DS basic research in the coming decade.

Data and code availability

The accession number for the WGS raw read data reported in this paper is DDBJ: DRA010895. All other data are available on request.

Supplemental information

Supplemental information can be found online at https://doi.org/10.1016/j.ajhg.2021.12.015.

Acknowledgments

We thank Toko Kurosaki, Yukako Sumida, Masami Morimura, Kei Yoshida, Eri Kaneda, Tomoko Ashiba, Megumi Hirose, Kazuomi Nakamura, Masato Takiguchi, Takashi Takeuchi, Manami Oka, Rina Ohnishi, and Michika Fukino at Tottori University and Kei Hiramatsu and Kayoko Morimoto at Trans Chromosomics, Inc. for their technical assistance; we also thank Hiroyuki Kugoh, Tetsuya Ohbayashi, Hiroyuki Satofuka, Takashi Moriwaki, and Takahito Ohira at Tottori University and Yoshihiro Oomiya at Health Research Institute, National Institute of Advanced Industrial Science and Technology (AIST) for critical discussions. This research was partly performed at the Tottori Bio Frontier managed by Tottori prefecture. The work was supported in part by JST CREST grant number JPMJCR18S4, Japan (Y.K.), a grant of General Collaborative Project from the National Institute for Physiological Sciences, Japan (NIPS; 17-252 to Y.K.), The Mitsubishi Foundation (M.O.), R01HD038384 (R.H.R), and R21HD098540 (R.H.R.).

Declaration of interests

M.O. is a CEO, employee, and shareholder of Trans Chromosomics, Inc., and S.A., H.T., and S.T. are employees of Trans Chromosomics, Inc. Other authors declare no conflicts of interest.

Received: October 6, 2021
Accepted: December 21, 2021
Published: January 24, 2022

References

1. Driscoll, D.A., and Gross, S. (2009). Clinical practice. Prenatal screening for aneuploidy. N. Engl. J. Med. *360*, 2556–2562.
2. Korenberg, J.R., Chen, X.N., Schipper, R., Sun, Z., Gonsky, R., Gerwehr, S., Carpenter, N., Daumer, C., Dignan, P., Disteche, C., et al. (1994). Down syndrome phenotypes: the consequences of chromosomal imbalance. Proc. Natl. Acad. Sci. USA *91*, 4997–5001.
3. Antonarakis, S.E., Skotko, B.G., Rafii, M.S., Strydom, A., Pape, S.E., Bianchi, D.W., Sherman, S.L., and Reeves, R.H. (2020). Down syndrome. Nat. Rev. Dis. Primers *6*, 9.

4. de Graaf, G., Buckley, F., and Skotko, B.G. (2017). Estimation of the number of people with Down syndrome in the United States. Genet. Med. *19*, 439–447.
5. Pritchard, M.A., and Kola, I. (1999). The "gene dosage effect" hypothesis versus the "amplified developmental instability" hypothesis in Down syndrome. J. Neural Transm. Suppl. *57*, 293–303.
6. Davisson, M.T., Schmidt, C., and Akeson, E.C. (1990). Segmental trisomy of murine chromosome 16: a new model system for studying Down syndrome. Prog. Clin. Biol. Res. *360*, 263–280.
7. Davisson, M.T., Schmidt, C., Reeves, R.H., Irving, N.G., Akeson, E.C., Harris, B.S., and Bronson, R.T. (1993). Segmental trisomy as a mouse model for Down syndrome. Prog. Clin. Biol. Res. *384*, 117–133.
8. Reeves, R.H., Irving, N.G., Moran, T.H., Wohn, A., Kitt, C., Sisodia, S.S., Schmidt, C., Bronson, R.T., and Davisson, M.T. (1995). A mouse model for Down syndrome exhibits learning and behaviour deficits. Nat. Genet. *11*, 177–184.
9. Moyer, A.J., Gardiner, K., and Reeves, R.H. (2021). All Creatures Great and Small: New Approaches for Understanding Down Syndrome Genetics. Trends Genet. *37*, 444–459.
10. Duchon, A., Raveau, M., Chevalier, C., Nalesso, V., Sharp, A.J., and Herault, Y. (2011). Identification of the translocation breakpoints in the Ts65Dn and Ts1Cje mouse lines: relevance for modeling Down syndrome. Mamm. Genome *22*, 674–684.
11. Reinholdt, L.G., Ding, Y., Gilbert, G.J., Czechanski, A., Solzak, J.P., Roper, R.J., Johnson, M.T., Donahue, L.R., Lutz, C., and Davisson, M.T. (2011). Molecular characterization of the translocation breakpoints in the Down syndrome mouse model Ts65Dn. Mamm. Genome *22*, 685–691.
12. Li, Z., Yu, T., Morishima, M., Pao, A., LaDuca, J., Conroy, J., Nowak, N., Matsui, S., Shiraishi, I., and Yu, Y.E. (2007). Duplication of the entire 22.9 Mb human chromosome 21 syntenic region on mouse chromosome 16 causes cardiovascular and gastrointestinal abnormalities. Hum. Mol. Genet. *16*, 1359–1366.
13. Yu, T., Li, Z., Jia, Z., Clapcote, S.J., Liu, C., Li, S., Asrar, S., Pao, A., Chen, R., Fan, N., et al. (2010). A mouse model of Down syndrome trisomic for all human chromosome 21 syntenic regions. Hum. Mol. Genet. *19*, 2780–2791.
14. O'Doherty, A., Ruf, S., Mulligan, C., Hildreth, V., Errington, M.L., Cooke, S., Sesay, A., Modino, S., Vanes, L., Hernandez, D., et al. (2005). An aneuploid mouse strain carrying human chromosome 21 with Down syndrome phenotypes. Science *309*, 2033–2037.
15. Kazuki, Y., Gao, F.J., Li, Y., Moyer, A.J., Devenney, B., Hiramatsu, K., Miyagawa-Tomita, S., Abe, S., Kazuki, K., Kajitani, N., et al. (2020). A non-mosaic transchromosomic mouse model of down syndrome carrying the long arm of human chromosome 21. eLife *9*, e56223.
16. Moore, T.J., Zhang, H., Anderson, G., and Alexander, G.C. (2018). Estimated Costs of Pivotal Trials for Novel Therapeutic Agents Approved by the US Food and Drug Administration, 2015-2016. JAMA Intern. Med. *178*, 1451–1457.
17. Wong, C.H., Siah, K.W., and Lo, A.W. (2019). Estimation of clinical trial success rates and related parameters. Biostatistics *20*, 273–286.
18. Braudeau, J., Delatour, B., Duchon, A., Pereira, P.L., Dauphinot, L., de Chaumont, F., Olivo-Marin, J.C., Dodd, R.H., Hérault, Y., and Potier, M.C. (2011). Specific targeting of the GABA-A receptor α5 subtype by a selective inverse agonist restores cognitive deficits in Down syndrome mice. J. Psychopharmacol. *25*, 1030–1042.
19. de la Torre, R., de Sola, S., Hernandez, G., Farré, M., Pujol, J., Rodriguez, J., Espadaler, J.M., Langohr, K., Cuenca-Royo, A., Principe, A., et al. (2016). Safety and efficacy of cognitive training plus epigallocatechin-3-gallate in young adults with Down's syndrome (TESDAD): a double-blind, randomised, placebo-controlled, phase 2 trial. Lancet Neurol. *15*, 801–810.
20. Zhu, P.J., Khatiwada, S., Cui, Y., Reineke, L.C., Dooling, S.W., Kim, J.J., Li, W., Walter, P., and Costa-Mattioli, M. (2019). Activation of the ISR mediates the behavioral and neurophysiological abnormalities in Down syndrome. Science *366*, 843–849.
21. Das, I., Park, J.M., Shin, J.H., Jeon, S.K., Lorenzi, H., Linden, D.J., Worley, P.F., and Reeves, R.H. (2013). Hedgehog agonist therapy corrects structural and cognitive deficits in a Down syndrome mouse model. Sci. Transl. Med. *5*, 201ra120.
22. Gao, F.J., Klinedinst, D., Fernandez, F.X., Cheng, B., Savonenko, A., Devenney, B., Li, Y., Wu, D., Pomper, M.G., and Reeves, R.H. (2021). Forebrain Shh overexpression improves cognitive function and locomotor hyperactivity in an aneuploid mouse model of Down syndrome and its euploid littermates. Acta Neuropathol. Commun. *9*, 137.
23. Gibbs, R.A., Weinstock, G.M., Metzker, M.L., Muzny, D.M., Sodergren, E.J., Scherer, S., Scott, G., Steffen, D., Worley, K.C., Burch, P.E., et al. (2004). Genome sequence of the Brown Norway rat yields insights into mammalian evolution. Nature *428*, 493–521.
24. Waterston, R.H., Lindblad-Toh, K., Birney, E., Rogers, J., Abril, J.F., Agarwal, P., Agarwala, R., Ainscough, R., Alexandersson, M., An, P., et al. (2002). Initial sequencing and comparative analysis of the mouse genome. Nature *420*, 520–562.
25. Adkins, R.M., Gelke, E.L., Rowe, D., and Honeycutt, R.L. (2001). Molecular phylogeny and divergence time estimates for major rodent groups: evidence from multiple genes. Mol. Biol. Evol. *18*, 777–791.
26. Baizer, J.S. (2014). Unique features of the human brainstem and cerebellum. Front. Hum. Neurosci. *8*, 202.
27. Ellenbroek, B., and Youn, J. (2016). Rodent models in neuroscience research: is it a rat race? Dis. Model. Mech. *9*, 1079–1087.
28. Do Carmo, S., and Cuello, A.C. (2013). Modeling Alzheimer's disease in transgenic rats. Mol. Neurodegener. *8*, 37.
29. Birling, M.C., Schaeffer, L., André, P., Lindner, L., Maréchal, D., Ayadi, A., Sorg, T., Pavlovic, G., and Hérault, Y. (2017). Efficient and rapid generation of large genomic variants in rats and mice using CRISMERE. Sci. Rep. *7*, 43331.
30. Kazuki, Y., Kobayashi, K., Hirabayashi, M., Abe, S., Kajitani, N., Kazuki, K., Takehara, S., Takiguchi, M., Satoh, D., Kuze, J., et al. (2019). Humanized UGT2 and CYP3A transchromosomic rats for improved prediction of human drug metabolism. Proc. Natl. Acad. Sci. USA *116*, 3072–3081.
31. Kazuki, Y., Hoshiya, H., Takiguchi, M., Abe, S., Iida, Y., Osaki, M., Katoh, M., Hiratsuka, M., Shirayoshi, Y., Hiramatsu, K., et al. (2011). Refined human artificial chromosome vectors for gene therapy and animal transgenesis. Gene Ther. *18*, 384–393.
32. Tomizuka, K., Yoshida, H., Uejima, H., Kugoh, H., Sato, K., Ohguma, A., Hayasaka, M., Hanaoka, K., Oshimura, M., and Ishida, I. (1997). Functional expression and germline transmission of a human chromosome fragment in chimaeric mice. Nat. Genet. *16*, 133–143.

33. Hirabayashi, M., and Hochi, S. (2011). Rat Embryonic Stem Cells: Establishment and Their Use for Transgenesis. IntechOpen, 397–410.
34. Hirabayashi, M., Kato, M., and Hochi, S. (2008). Factors affecting full-term development of rat oocytes microinjected with fresh or cryopreserved round spermatids. Exp. Anim. *57*, 401–405.
35. Shinohara, T., Tomizuka, K., Miyabara, S., Takehara, S., Kazuki, Y., Inoue, J., Katoh, M., Nakane, H., Iino, A., Ohguma, A., et al. (2001). Mice containing a human chromosome 21 model behavioral impairment and cardiac anomalies of Down's syndrome. Hum. Mol. Genet. *10*, 1163–1175.
36. Lele, S.R., and Richtsmeier, J.T. (2001). An Invariant Approach to Statistical Analysis of Shapes (Chapman and Hall/CRC).
37. Richtsmeier, J.T., and Lele, S. (1993). A coordinate-free approach to the analysis of growth patterns: models and theoretical considerations. Biol. Rev. Camb. Philos. Soc. *68*, 381–411.
38. Lele, S., and Richtsmeier, J.T. (1995). Euclidean distance matrix analysis: confidence intervals for form and growth differences. Am. J. Phys. Anthropol. *98*, 73–86.
39. Rohlf, F.J., and Slice, D. (1990). Extensions of the Procrustes Method for the Optimal Superimposition of Landmarks. Syst. Zool. *39*, 40–59.
40. Slice, D.E. (2007). Geometric morphometrics. Annu. Rev. Anthropol. *36*, 261–281.
41. Inoue, J., Mitsuya, K., Maegawa, S., Kugoh, H., Kadota, M., Okamura, D., Shinohara, T., Nishihara, S., Takehara, S., Yamauchi, K., et al. (2001). Construction of 700 human/mouse A9 monochromosomal hybrids and analysis of imprinted genes on human chromosome 6. J. Hum. Genet. *46*, 137–145.
42. Gupta, M., Dhanasekaran, A.R., and Gardiner, K.J. (2016). Mouse models of Down syndrome: gene content and consequences. Mamm. Genome *27*, 538–555.
43. Saran, N.G., Pletcher, M.T., Natale, J.E., Cheng, Y., and Reeves, R.H. (2003). Global disruption of the cerebellar transcriptome in a Down syndrome mouse model. Hum. Mol. Genet. *12*, 2013–2019.
44. Do, C., Xing, Z., Yu, Y.E., and Tycko, B. (2017). Trans-acting epigenetic effects of chromosomal aneuploidies: lessons from Down syndrome and mouse models. Epigenomics *9*, 189–207.
45. Letourneau, A., Santoni, F.A., Bonilla, X., Sailani, M.R., Gonzalez, D., Kind, J., Chevalier, C., Thurman, R., Sandstrom, R.S., Hibaoui, Y., et al. (2014). Domains of genome-wide gene expression dysregulation in Down's syndrome. Nature *508*, 345–350.
46. Shinohara, T., Tomizuka, K., Takehara, S., Yamauchi, K., Katoh, M., Ohguma, A., Ishida, I., and Oshimura, M. (2000). Stability of transferred human chromosome fragments in cultured cells and in mice. Chromosome Res. *8*, 713–725.
47. Takiguchi, M., Kazuki, Y., Hiramatsu, K., Abe, S., Iida, Y., Takehara, S., Nishida, T., Ohbayashi, T., Wakayama, T., and Oshimura, M. (2014). A novel and stable mouse artificial chromosome vector. ACS Synth. Biol. *3*, 903–914.
48. Wilson, M.D., Barbosa-Morais, N.L., Schmidt, D., Conboy, C.M., Vanes, L., Tybulewicz, V.L., Fisher, E.M., Tavaré, S., and Odom, D.T. (2008). Species-specific transcription in mice carrying human chromosome 21. Science *322*, 434–438.
49. Takao, K., and Miyakawa, T. (2006). Light/dark transition test for mice. J. Vis. Exp. *1*, 104.
50. Arrant, A.E., Schramm-Sapyta, N.L., and Kuhn, C.M. (2013). Use of the light/dark test for anxiety in adult and adolescent male rats. Behav. Brain Res. *256*, 119–127.
51. Crusio, W.E. (2001). Genetic dissection of mouse exploratory behaviour. Behav. Brain Res. *125*, 127–132.
52. Feyissa, D.D., Aher, Y.D., Engidawork, E., Höger, H., Lubec, G., and Korz, V. (2017). Individual Differences in Male Rats in a Behavioral Test Battery: A Multivariate Statistical Approach. Front. Behav. Neurosci. *11*, 26.
53. Sun, T., and Hevner, R.F. (2014). Growth and folding of the mammalian cerebral cortex: from molecules to malformations. Nat. Rev. Neurosci. *15*, 217–232.
54. Baxter, L.L., Moran, T.H., Richtsmeier, J.T., Troncoso, J., and Reeves, R.H. (2000). Discovery and genetic localization of Down syndrome cerebellar phenotypes using the Ts65Dn mouse. Hum. Mol. Genet. *9*, 195–202.
55. Powell, N.M., Modat, M., Cardoso, M.J., Ma, D., Holmes, H.E., Yu, Y., O'Callaghan, J., Cleary, J.O., Sinclair, B., Wiseman, F.K., et al. (2016). Fully-Automated μMRI Morphometric Phenotyping of the Tc1 Mouse Model of Down Syndrome. PLoS ONE *11*, e0162974.
56. Pinter, J.D., Eliez, S., Schmitt, J.E., Capone, G.T., and Reiss, A.L. (2001). Neuroanatomy of Down's syndrome: a high-resolution MRI study. Am. J. Psychiatry *158*, 1659–1665.
57. Ferencz, C., Neill, C.A., Boughman, J.A., Rubin, J.D., Brenner, J.I., and Perry, L.W. (1989). Congenital cardiovascular malformations associated with chromosome abnormalities: an epidemiologic study. J. Pediatr. *114*, 79–86.
58. Chapman, R.S., and Hesketh, L.J. (2000). Behavioral phenotype of individuals with Down syndrome. Ment. Retard. Dev. Disabil. Res. Rev. *6*, 84–95.
59. Stores, R., Stores, G., Fellows, B., and Buckley, S. (1998). Daytime behaviour problems and maternal stress in children with Down's syndrome, their siblings, and non-intellectually disabled and other intellectually disabled peers. J. Intellect. Disabil. Res. *42*, 228–237.
60. Ekstein, S., Glick, B., Weill, M., Kay, B., and Berger, I. (2011). Down syndrome and attention-deficit/hyperactivity disorder (ADHD). J. Child Neurol. *26*, 1290–1295.
61. Oxelgren, U.W., Myrelid, Å., Annerén, G., Ekstam, B., Göransson, C., Holmbom, A., Isaksson, A., Åberg, M., Gustafsson, J., and Fernell, E. (2017). Prevalence of autism and attention-deficit-hyperactivity disorder in Down syndrome: a population-based study. Dev. Med. Child Neurol. *59*, 276–283.
62. Faizi, M., Bader, P.L., Tun, C., Encarnacion, A., Kleschevnikov, A., Belichenko, P., Saw, N., Priestley, M., Tsien, R.W., Mobley, W.C., and Shamloo, M. (2011). Comprehensive behavioral phenotyping of Ts65Dn mouse model of Down syndrome: activation of β1-adrenergic receptor by xamoterol as a potential cognitive enhancer. Neurobiol. Dis. *43*, 397–413.
63. Kleschevnikov, A.M., Belichenko, P.V., Faizi, M., Jacobs, L.F., Htun, K., Shamloo, M., and Mobley, W.C. (2012). Deficits in cognition and synaptic plasticity in a mouse model of Down syndrome ameliorated by GABAB receptor antagonists. J. Neurosci. *32*, 9217–9227.
64. Galante, M., Jani, H., Vanes, L., Daniel, H., Fisher, E.M., Tybulewicz, V.L., Bliss, T.V., and Morice, E. (2009). Impairments in motor coordination without major changes in cerebellar plasticity in the Tc1 mouse model of Down syndrome. Hum. Mol. Genet. *18*, 1449–1463.

65. Papavassiliou, P., Charalsawadi, C., Rafferty, K., and Jackson-Cook, C. (2015). Mosaicism for trisomy 21: a review. Am. J. Med. Genet. A. *167A*, 26–39.
66. Bornstein, E., Lenchner, E., Donnenfeld, A., Kapp, S., Keeler, S.M., and Divon, M.Y. (2009). Comparison of modes of ascertainment for mosaic vs complete trisomy 21. Am. J. Obstet. Gynecol. *200*, 440.e1–440445.
67. Zhao, W., Chen, F., Wu, M., Jiang, S., Wu, B., Luo, H., Wen, J., Hu, C., and Yu, S. (2015). Postnatal Identification of Trisomy 21: An Overview of 7,133 Postnatal Trisomy 21 Cases Identified in a Diagnostic Reference Laboratory in China. PLoS ONE *10*, e0133151.
68. Devlin, L., and Morrison, P.J. (2004). Accuracy of the clinical diagnosis of Down syndrome. Ulster Med. J. *73*, 4–12.
69. Ponomartsev, S.V., Sinenko, S.A., Skvortsova, E.V., Liskovykh, M.A., Voropaev, I.N., Savina, M.M., Kuzmin, A.A., Kuzmina, E.Y., Kondrashkina, A.M., Larionov, V., et al. (2020). Human Alphoid(tetO) Artificial Chromosome as a Gene Therapy Vector for the Developing Hemophilia A Model in Mice. Cells *9*, 879.
70. Zhu, F., Nair, R.R., Fisher, E.M.C., and Cunningham, T.J. (2019). Humanising the mouse genome piece by piece. Nat. Commun. *10*, 1845.
71. Tomizuka, K., Shinohara, T., Yoshida, H., Uejima, H., Ohguma, A., Tanaka, S., Sato, K., Oshimura, M., and Ishida, I. (2000). Double trans-chromosomic mice: maintenance of two individual human chromosome fragments containing Ig heavy and kappa loci and expression of fully human antibodies. Proc. Natl. Acad. Sci. USA *97*, 722–727.
72. Wu, D., Zhang, Y., Cheng, B., Mori, S., Reeves, R.H., and Gao, F.J. (2021). Time-dependent diffusion MRI probes cerebellar microstructural alterations in a mouse model of Down syndrome. Brain Commun. *3*, fcab062.